Ab initio coupled-cluster calculations of ground and dipole excited states in ^{8}He

F. Bonaiti,[1] S. Bacca,[1,2] and G. Hagen[3,4]

[1]*Institut für Kernphysik and PRISMA^{+} Cluster of Excellence, Johannes Gutenberg-Universität, 55128 Mainz, Germany*
[2]*Helmholtz-Institut Mainz, Johannes Gutenberg-Universität Mainz, D-55099 Mainz, Germany*
[3]*Physics Division, Oak Ridge National Laboratory, Oak Ridge, Tennessee 37831, USA*
[4]*Department of Physics and Astronomy, University of Tennessee, Knoxville, Tennessee 37996, USA*

(Received 16 December 2021; accepted 18 February 2022; published 10 March 2022)

We perform coupled-cluster calculations of ground- and dipole excited-state properties of the ^{8}He halo nucleus with nucleon-nucleon and three-nucleon interactions from chiral effective field theory, both with and without explicit delta degrees of freedom. By increasing the precision in our coupled-cluster calculations via the inclusion of leading-order three-particle three-hole excitations in the cluster operator, we obtain a ground-state energy and a charge radius that are consistent with experiment, albeit with a slight underbinding. We also investigate the excited states induced by the electric dipole operator and present a discussion on the Thomas-Reiche-Kuhn and cluster sum rules. Finally, we compute the electric dipole polarizability, providing a theoretical benchmark for future experimental determinations that will study this exotic nucleus.

DOI: 10.1103/PhysRevC.105.034313

I. INTRODUCTION

Light nuclei close to the driplines exhibit fascinating phenomena, such as the formation of diluted structures where a tightly bound core is surrounded by a halo of one or more weakly bound nucleons. Signatures for halo structures are both a small separation energy and a large matter radius, that does not follow the typical $A^{1/3}$ behavior characterizing stable nuclei. Since their discovery in the 1980s [1,2], halo nuclei have attracted a lot of attention in the nuclear physics community, both from the experimental and the theoretical point of view. While from the experimental side enormous progress has been made and precision measurements of masses and radii are nowadays possible even for very short lived systems (see, e.g., Ref. [3]), halo nuclei still represent an arduous task for nuclear theory. The reason lies in their extended size, which challenges several of the available many-body methods.

The helium isotope chain is particularly interesting in terms of the physics of halo nuclei. The chain presents an unbound-bound staggering when adding an odd-even number of neutrons on top of ^{4}He: ^{5}He is unbound, ^{6}He is a bound halo nucleus, ^{7}He is unbound, and ^{8}He is again a bound halo nucleus. Of the two halo nuclei, ^{6}He is a borromean halo system [4], and ^{8}He is the only known four-neutron halo nucleus. Both ^{6}He and ^{8}He have already been extensively investigated in the literature also with the so-called *ab initio* methods (see, e.g., Refs. [5–12]).

In this paper, we will focus on the ^{8}He halo nucleus and present a study based on the *ab initio* coupled-cluster (CC) method [13–19]. Two reasons motivate this analysis. On the one hand, ^{8}He can be seen as the most exotic nucleus having the largest neutron-to-proton ratio across the nuclear chart ($N/Z = 3$), and as such it is interesting to test the models of nuclear forces developed in the *ab initio* community on this nucleus. On the other hand, there have been some recent updates on the experimental determinations of the ^{8}He ground-state properties, for example of its charge radius [20], and measurements of its excitation spectrum have either been made [12] or are being planned [21]. Hence, new calculations based on the most modern interactions and many-body methods are interesting.

Our starting point to describe the nucleus of ^{8}He is the intrinsic nuclear Hamiltonian

$$H = \frac{1}{2mA}\sum_{i<j}^{A}(\vec{p}_i - \vec{p}_j)^2 + \sum_{i<j}^{A} V_{ij} + \sum_{i<j<k}^{A} W_{ijk}, \qquad (1)$$

where m is the nucleon mass, $A = 8$ is the mass number, V_{ij} is the two-body force, and W_{ijk} is the three-body force. In the last years, a lot of progress has been achieved in deriving two- and three-body forces from chiral effective field theory (χEFT) [22–24], and different optimization strategies have been implemented for the low-energy constants (LECs) [25,26]. In particular, chiral interactions with explicit delta degrees of freedom are also becoming available [27–32]. In this paper we will explore both delta-full and delta-less interactions in our computations of ^{8}He.

We will focus on ground-state properties such as the binding energy and the charge radius, and on the low-energy excited states of dipole nature. For the latter, we will perform calculations based on a method that merges the Lorentz integral transform (LIT) with CC theory, called LIT-CC [33,34]. This approach has already proved to be successful in capturing properties of unstable neutron-rich nuclei, such as ^{22}O in Ref. [34], where the pygmy dipole resonance was reproduced using a chiral two-body interaction. With respect to Ref. [34], we now have the advantage that we are able to include

three-nucleon forces and effects of triples correlations in the CC expansion [35].

The paper is organized as follows. In Sec. II, a description of our theoretical approach is provided. In Sec. III, we present an overview of our results, separating the ground-state observables from the dipole excited-state properties. For the latter we devote one subsection to the energy-weighted sum rule and one subsection to the electric dipole polarizability. In Sec. IV, we draw our conclusions.

II. COMPUTATIONAL TOOLS

For a given nuclear Hamiltonian H, the CC approach is based on an exponential ansatz for the nuclear many-body wave function:

$$|\Psi_0\rangle = e^T |\Phi_0\rangle. \tag{2}$$

Here, $|\Phi_0\rangle$ is a reference Slater determinant state, typically obtained from a Hartree-Fock calculation, where single-particle states are projected onto the harmonic oscillator (HO) basis. The cluster operator T introduces correlations in the many-body wave function, and can be expanded in terms of n-particle n-hole excitations as

$$T = T_1 + T_2 + T_3 + \cdots + T_A. \tag{3}$$

The Schrödinger equation for the ground state of an A-particle system can be rewritten in the following form:

$$\overline{H}_N |\Phi_0\rangle = E_0 |\Phi_0\rangle, \tag{4}$$

where

$$\overline{H}_N = e^{-T} H_N e^T \tag{5}$$

is the similarity-transformed Hamiltonian obtained starting from H_N, which is the normal-ordered Hamiltonian of Eq. (1) with respect to the reference $|\Phi_0\rangle$. In this paper we use the normal-ordered Hamiltonian in the two-body approximation [36,37]. Since the similarity-transformed Hamiltonian is non-Hermitian, the calculation of expectation values in CC theory requires the knowledge of both the left and right eigenstates. The right ground state is given by $|0\rangle = |\Phi_0\rangle$, while the left ground state is

$$\langle 0| = \langle \Phi_0|(1 + \Lambda), \quad \Lambda = \Lambda_1 + \Lambda_2 + \ldots, \tag{6}$$

where the operator Λ is expanded as a sum of particle-hole deexcitation operators.

Our goal is to study also the dipole excitation of ^{8}He and related sum rules. For this purpose, we first introduce the dipole response function

$$R(\omega) = \sum_\mu |\langle \Psi_\mu | \Theta | \Psi_0 \rangle|^2 \delta(E_\mu - E_0 - \omega), \tag{7}$$

where $|\Psi_\mu\rangle$ are the excited states connected to the ground state by the dipole operator Θ, and ω is the photon energy. The dipole operator is given by

$$\Theta = \sum_k^A (\mathbf{r}_k - \mathbf{R}_{\text{c.m.}}) \left(\frac{1 + \tau_k^3}{2} \right), \tag{8}$$

where $\mathbf{r}_k$ and $\mathbf{R}_{\text{c.m.}}$ are the coordinates of the kth nucleon and the center of mass, respectively, while τ_k^3 is the third component of the isospin operator.

Due to the non-Hermitian nature of the similarity transformed Hamiltonian, also for the excited states we have to distinguish between right and left eigenstates of the Hamiltonian. The latter are obtained using the CC equation-of-motion (EOM) method [38] and are defined as

$$\begin{aligned} \overline{H}_N R_\mu |\Phi_0\rangle &= E_\mu R_\mu |\Phi_0\rangle, \\ \langle \Phi_0 | L_\mu \overline{H}_N &= E_\mu \langle \Phi_0 | L_\mu, \end{aligned} \tag{9}$$

where the operators R_μ and L_μ are expressed in terms of a linear combination of particle-hole excitations as well.

Using Eqs. (6) and (9), we can write the response function corresponding to the similarity-transformed Hamiltonian as

$$\begin{aligned} R(\omega) = \sum_\mu &\langle \Phi_0 | (1 + \Lambda) \overline{\Theta}_N^\dagger R_\mu | \Phi_0 \rangle \langle \Phi_0 | L_\mu \overline{\Theta}_N | \Phi_0 \rangle \\ &\times \delta(E_\mu - E_0 - \omega) \end{aligned} \tag{10}$$

where

$$\overline{\Theta}_N = e^{-T} \Theta_N e^T \tag{11}$$

is the similarity transformed transition operator. It is important to observe that the sum over μ in $R(\omega)$ corresponds to both a sum over discrete excited states and an integral over continuum eigenstates of the Hamiltonian. In particular, the calculation of the latter represents a formidable task. Continuum state wave functions, in fact, contain information about all the possible fragmentation channels of the nucleus at a given energy. To avoid the issue of explicitly computing the states in the continuum, we merged the CC method with the LIT technique [39,40], originally used in few-body calculations. This led to the development of the so-called LIT-CC method, where the calculation of an integral transform of $R(\omega)$ with Lorentzian kernel

$$L(\sigma, \Gamma) = \frac{\Gamma}{\pi} \int d\omega \, \frac{R(\omega)}{(\omega - \sigma)^2 + \Gamma^2} \tag{12}$$

is directly related to the CC equation-of-motion method with a source term [33,34]. Once $L(\sigma, \Gamma)$ is calculated, a numerical inversion procedure allows one to recover $R(\omega)$ (see Ref. [40] for details).

Starting from the LIT, one can easily obtain an estimate of the electromagnetic sum rules, i.e., the moments of the response function interpreted as a distribution function. Knowing all the moments is equivalent to knowing the distribution itself. However, it is sometimes easier to compute just a few moments of a distribution rather than the full distribution, and yet obtain substantial insights into the dynamics of a quantum system.

The moments (or sum rules) of the response function are defined as

$$m_n = \int d\omega \, \omega^n R(\omega), \tag{13}$$

where n is an integer. Because in the limit $\Gamma \to 0$ the Lorentzian kernel becomes a delta function, we have that

$$L(\sigma, \Gamma \to 0) = \int d\omega\, R(\omega)\delta(\omega - \sigma) = R(\sigma), \tag{14}$$

i.e., the moments can be computed from the LIT as

$$m_n = \int d\sigma\, \sigma^n L(\sigma, \Gamma \to 0). \tag{15}$$

As shown in Ref. [41], this method is equivalent to obtaining first $R(\omega)$ and then integrating it, with the advantage that one does not have to perform an inversion, a procedure which can add to the total numerical error budget. In this paper, we will focus on the calculation of two dipole sum rules: the energy-weighted m_1 and the inverse-energy weighted m_{-1}.

III. RESULTS

In this paper we aim at performing a systematic study of the ground- and dipole excited-state properties of ^{8}He, supported by a reliable estimate of our theoretical uncertainties. Our computations are affected mainly by three sources of uncertainties: (i) the model space truncation, (ii) the many-body truncation, and (iii) the dependence on the employed interaction model.

In order to address (i), we need to take into account the fact that the expansion on the model space is controlled by the maximum number of HO shells $N_{\max}$ included in the calculation, for a given HO frequency $\hbar\Omega$. For sufficiently large $N_{\max}$ the results should be virtually independent of the choice of $\hbar\Omega$. In this paper, we use $N_{\max} = 14, 16$ and use the small residual $\hbar\Omega$ dependence (varying $\hbar\Omega$ in the range 12–16 MeV) as a way to assess the uncertainty in the model space truncation.

In CC theory the particle-hole expansion of the cluster operator is truncated due to computational limitations. To address (ii) in this paper we explore the effect of the CC truncation on both the ground and the excited states. In computing ground-state properties, the most frequently adopted approximation is CC with singles and doubles excitations, corresponding to $T = T_1 + T_2$ and $\Lambda = \Lambda_1 + \Lambda_2$. We will denote this truncation scheme with D. Next, we will also analyze results obtained by including leading-order $3p$-$3h$ excitations, which we denote here with T-1 [42]. In calculating excited-state observables, we will also make two choices for the approximation level of the EOM computation, either D or T-1 [43,44]. Since the calculation of the dipole response functions and sum rules require us to perform a particle-hole expansion for the ground state (T and Λ), and a corresponding one for the EOM computation of the excited states (R_μ and L_μ), we indicate two expansion schemes. The resulting CC truncation schemes for the dipole sum rule calculation are listed in Table I. We estimate the uncertainty (ii) at the optimal HO frequency $\hbar\Omega$ by computing the difference between the results obtained with two CC schemes.

Finally, to address (iii), we compare the results obtained using three different chiral EFT interactions: NNLO$_{\rm sat}$[26] and the Δ-full interactions ΔNNLO$_{\rm GO}$(394) and ΔNNLO$_{\rm GO}$(450) [32]. These interactions are all given at next-to-next-to-leading order in the chiral expansion, and include three-body forces. It is worth noticing that the two Δ-full interactions differ just by the value of the cutoff, which is 394 and 450 MeV/c for ΔNNLO$_{\rm GO}$(394) and ΔNNLO$_{\rm GO}$(450), respectively. Employing these three different chiral interaction models enables us to appreciate the effect of including explicit delta isobars, varying the cutoff and the employed optimization protocol used for the LECs on the observables under analysis. A rigourous order-by-order treatment of χEFT uncertainty is left for future work.

TABLE I. List of labels used to identify the CC truncation for the ground state (left of the solidus) and the excited state (right of the solidus). Note that for Eq. (11), we include only up to $2p$-$2h$ excitations in the T, as the effect of triples corrections is negligible [35].

Ground state	EOM calculation	Truncation scheme
D	D	D/D
T-1	D	T-1/D
T-1	T-1	T-1/T-1

In the results we will display in this section, the uncertainties stemming from (i) and (ii) are added in quadrature, following Ref. [45]. Regarding (iii), we work with three interactions and present them separately in tables and figures.

A. Ground-state properties

We start by presenting CC results for the ground-state energy $E_{\rm GS}$ of ^{8}He. While $E_{\rm GS}$ was already obtained from coupled-cluster theory using the NNLO$_{\rm sat}$ interaction in Ref. [26], in this paper we further extend the analysis by showing the convergence with respect to the CC truncation, $N_{\max}$ and $\hbar\Omega$, and by comparing the results from NNLO$_{\rm sat}$ with those from ΔNNLO$_{\rm GO}$(394) and ΔNNLO$_{\rm GO}$(450).

The model space convergence for $E_{\rm GS}$ with a comparison to experimental data is shown in Fig. 1, for the D and T-1 truncation schemes. At the optimal frequency $\hbar\Omega = 16$ MeV, the ground-state energy values are converged with respect to $N_{\max}$ for all three interactions. In the case of the Δ-full interactions it is interesting to discuss the effect of the different values of the cutoff on the $\hbar\Omega$ dependence: while the ΔNNLO$_{\rm GO}$(394) results for $\hbar\Omega = 12$ and 16 MeV are fully overlapped, for ΔNNLO$_{\rm GO}$(450) the dependence on the HO frequency remains apparent. This is expected, as the higher cutoff leads to a harder interaction. The role of triples corrections is crucial in bringing theory closer to experiment. For all the interactions, $3p$-$3h$ excitations represent between 8 and 9% of the CCSD correlation energy, moving our theoretical results in the direction of the experimental value. The final outcomes for the ground-state energy are reported in Table II. We remark that the uncertainty, obtained summing (i) and (ii) in quadrature, is dominated by the CC truncation. The NNLO$_{\rm sat}$ interaction gives the best agreement with respect to the experimental energy. We note that it has recently been shown that ^{8}He is soft towards being deformed in its ground state [11,12]. The static correlations associated with deformation are not accurately captured in our spherical CC approach,

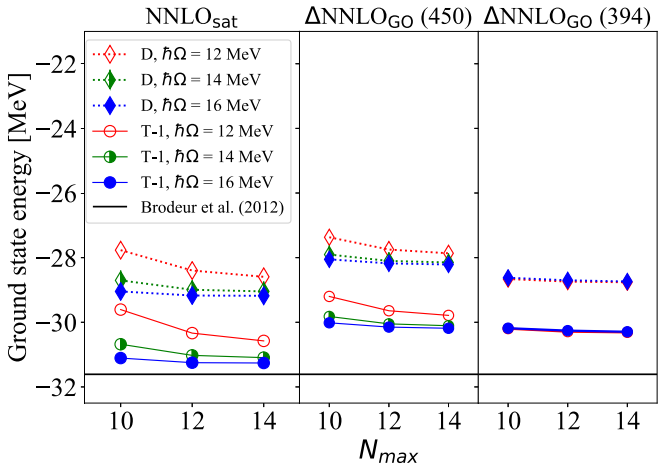

FIG. 1. Ground-state energy of ^{8}He in the D and T-1 scheme as a function of the model-size $N_{\max}$ for the three Hamiltonians. The experimental value of the ground-state energy is taken from Ref. [46].

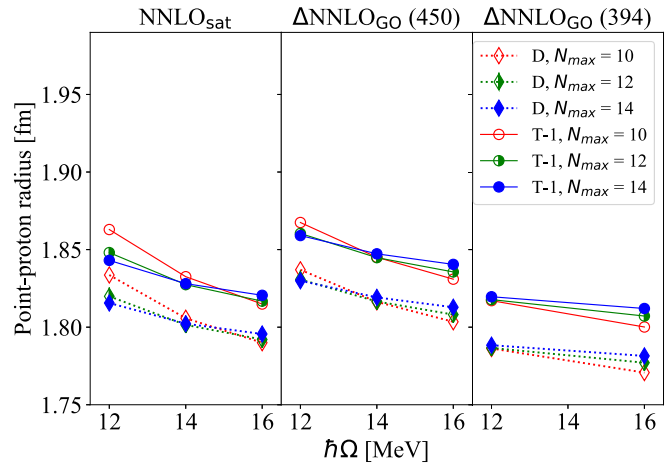

FIG. 2. Point-proton radius of ^{8}He in the D and T-1 scheme as a function of the HO frequency $\hbar\Omega$ for the three Hamiltonians.

and this might explain the slight underbinding we find for ΔNNLO$_{\rm GO}$(450) and ΔNNLO$_{\rm GO}$(394). Next we turn to our results for the charge radius of ^{8}He. In order to analyze the nuclear charge radius $R_{\rm ch}$, we first compute the point-proton radius R_{pp}. Coupled-cluster results of R_{pp} as a function of $\hbar\Omega$ are shown in Fig. 2, for the D and T-1 truncation schemes. For each interaction, we identify the optimal frequency, leading to the best convergence as a function of the model space size, with the crossing point of the curves characterized by different $N_{\max}$. In particular, for NNLO$_{\rm sat}$ and ΔNNLO$_{\rm GO}$(450) (both with cutoff of 450 MeV/c) the optimal frequency is $\hbar\Omega =$ 14 MeV, while for ΔNNLO$_{\rm GO}$(394) the optimal frequency is 12 MeV. As in the case of the ground-state energy, we see that the cutoff affects the $\hbar\Omega$ dependence of our results, leading to a faster convergence when the cutoff is lower. Moreover, we notice that the effect of triples corrections for R_{pp} is smaller than in the case of $E_{\rm GS}$. At the optimal frequency, in fact, the difference between the R_{pp} values for D and T-1 amounts to around 1.5% for all interactions.

Starting from R_{pp}, we then compute the charge radius using

$$\langle R^2_{\rm ch}\rangle = \langle R^2_{pp}\rangle + R^2_p + \frac{N}{Z}R^2_n + \frac{3}{4M^2_p} + R^2_{\rm SO}, \qquad (16)$$

where $R_p = 0.8414(19)$ fm [47] is the proton charge radius, $R^2_n = -0.106^{+0.007}_{-0.005}$ fm^2 [48] is the neutron charge radius, $3/(4M_p^2) = 0.033$ fm^2 is the Darwin-Foldy term, and $R^2_{\rm SO}$ is the spin-orbit correction. In Ref. [49] it has been pointed out that $R^2_{\rm SO}$ could give a remarkable contribution to the charge radius of halo nuclei. Therefore, we have consistently calculated this correction in CC theory, improving in this respect Ref. [26]. Our results are reported in Table III, in comparison to previous theoretical estimates. Also in this case the uncertainties are obtained by summing in quadrature (i) and (ii). The prediction of Ref. [49] is based on a shell model calculation, while in Ref. [50] the complex-energy configuration interaction method is employed. In this framework, the CC approach allows us to account for many-body correlations, leading to a significant improvement with respect to previous calculations of this quantity. In fact, in CC the magnitude of $R^2_{\rm SO}$ is reduced by about 10% with respect to Ref. [50], and by approximately 20% with respect to the shell model estimate.

The final results for the charge radius of ^{8}He are illustrated in Fig. 3 in comparison to three experimental determinations. The charge radius of ^{8}He can be experimentally obtained from a measurement of the isotope shift, namely, the frequency difference $\delta\nu_{\rm A,A'}$ between ^{8}He and the reference isotope ^{4}He, in the same atomic transition. The frequency shift is related to the difference $\delta\langle R^2_{\rm ch}\rangle_{\rm A,A'}$ in the charge radius between ^{8}He and ^{4}He by

$$\delta\nu_{\rm A,A'} = \delta^{\rm mass}_{\rm A,A'} + K_{\rm FS}\delta\langle R^2_{\rm ch}\rangle_{\rm A,A'}, \qquad (17)$$

TABLE II. Theoretical predictions for the ground-state energy of ^{8}He in MeV for the three different interactions in comparison to experiment.

Interaction	Ground-state energy
NNLO$_{\rm sat}$	−31(1)
ΔNNLO$_{\rm GO}$(450)	−30(1)
ΔNNLO$_{\rm GO}$(394)	−30.3(8)
Experiment [46]	−31.60972(11)

TABLE III. Theoretical predictions for the spin-orbit correction to the charge radius of ^{8}He for the three different interactions in comparison to previous theoretical results.

Interaction	$R^2_{\rm SO}$ (fm^2)
NNLO$_{\rm sat}$	−0.143(6)
ΔNNLO$_{\rm GO}$(450)	−0.134(9)
ΔNNLO$_{\rm GO}$(394)	−0.141(6)
Ref. [49]	−0.17
Ref. [50]	−0.158

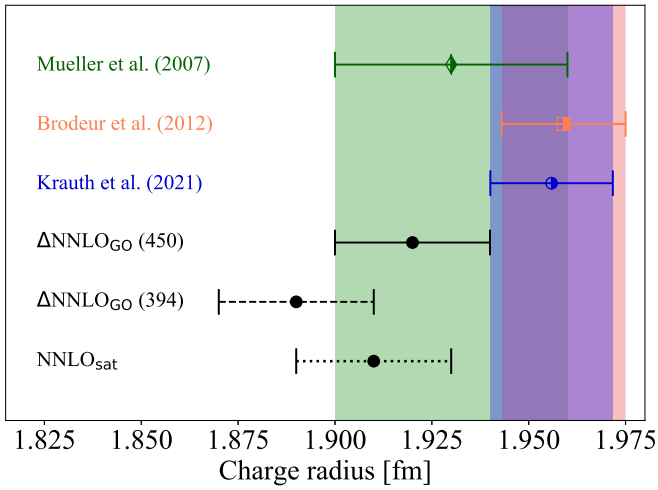

FIG. 3. Comparison between the coupled-cluster theoretical values for the charge radius of ^{8}He using the three different Hamiltonians and the experimental results of Mueller *et al.* [51], Brodeur *et al.* [46], and Krauth *et al.* [20].

where the mass shift $\delta^{\text{mass}}_{A,A'}$ and the field shift constant K_{FS} are obtained from precise atomic theory calculations. The first determination of the charge radius of ^{8}He using this method stems from Ref. [51], where the radius of ^{4}He measured from electron scattering was used as a reference. Later, Ref. [46] provided an improved estimate of the mass and field shift parameters, based on precise nuclear mass measurements. More recently, Ref. [20] achieved the first determination of the ^{4}He charge radius from muonic atoms, which, improving the reference, slightly modified the R_{ch} for ^{8}He.

In general, we find that our theoretical results are in good accordance with the experimental determinations, as seen in Fig. 3. In particular, the ΔNNLO$_{\text{GO}}$(450) interaction leads to the largest charge radius, equal to 1.92(2) fm, which agrees best with Ref. [51]. The larger radius is due to the interplay between the higher value for R_{pp} and the smaller value of R^2_{SO} obtained with this interaction in comparison to the other two. Moreover, the distance between the upper end of the ΔNNLO$_{\text{GO}}$(450) error bar and the lower end of that of the most recent experimental determination [20] amounts to 10^{-4} fm. Comparing this to the scale of the values involved, we can still claim a good agreement between these two results.

B. Discretized dipole response function and energy-weighted sum rule

We now address the dipole excited states in ^{8}He by first looking at the discretized response function. In our framework, this quantity can be simply calculated taking the limit of the LIT for $\Gamma \to 0$, as shown in Eq. (14). In Fig. 4, we show the LIT with $\Gamma = 10^{-4}$ MeV for the three different interactions. For all the potentials, the discretized response function presents low-energy peaks emerging at around 5 MeV. On the one hand, our results are consistent with the analysis of the ^{3}H(^{6}He, p)^{8}He transfer reaction in Ref. [52] where a low-lying dipole strength around 3 MeV was indicated. On the other hand, the recent inelastic proton scattering experiment

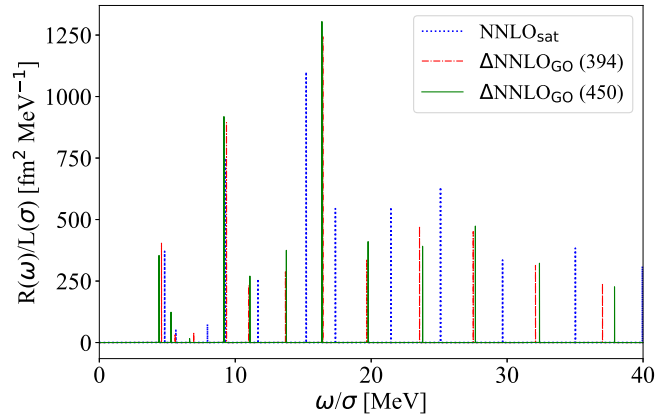

FIG. 4. Discretized response function of ^{8}He with $\Gamma = 10^{-4}$ MeV in the T-1/T-1 scheme for the different chiral EFT interactions.

on ^{8}He [12] did not observe any low-lying dipole resonance below 5 MeV. The larger number of states that we observe at about 20 MeV for all three interactions correspond to the giant dipole resonance.

Starting from the discretized response function and using Eq. (15), we can study the energy-weighted dipole sum rule m_1. Figure 5 illustrates its behavior as a function of $\hbar\Omega$ for various N_{max} in the D/D and T-1/T-1 truncation scheme. At a first glance, we immediately notice that the energy-weighted sum rule converges quite quickly. In the case of m_1, the largest contribution to the integral of Eq. (15) is represented by the high-energy dipole-excited states, which are well converged. It is interesting to look at the effect of varying the interaction cutoff on the $\hbar\Omega$ convergence pattern: while for NNLO$_{\text{sat}}$ and ΔNNLO$_{\text{GO}}$(450) we achieve a negligible dependence on N_{max} at $\hbar\Omega = 14$ MeV, in the case of ΔNNLO$_{\text{GO}}$(394) the optimal frequency corresponds to $\hbar\Omega = 12$ MeV.

The contribution of triples, going from the D/D to the T-1/T-1 truncation scheme is substantial and amounts to

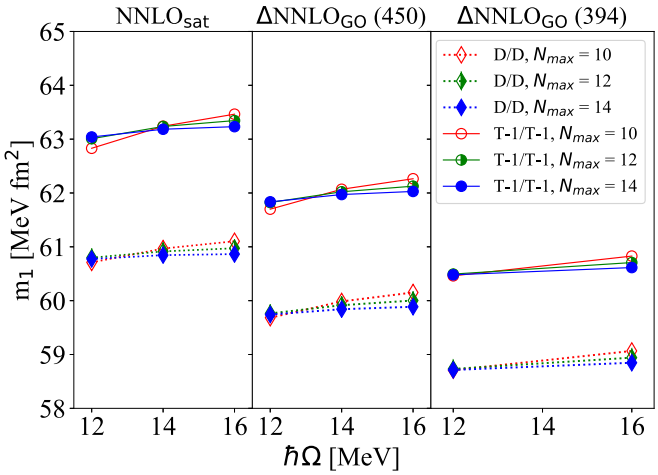

FIG. 5. Energy-weighted dipole sum rule for ^{8}He as a function of $\hbar\Omega$ for the three Hamiltonians in the D/D and T-1/T-1 truncation scheme.

TABLE IV. Theoretical predictions for the energy-weighted dipole sum rule of ^{8}He and the enhancement factor for the three different chiral EFT interactions under consideration.

Interaction	m_1 (MeV fm^2)	κ
NNLO$_{\rm sat}$	63(1)	1.02(3)
ΔNNLO$_{\rm GO}$(450)	62(1)	1.00(3)
ΔNNLO$_{\rm GO}$(394)	60.5(9)	0.94(3)

3.5% for NNLO$_{\rm sat}$ and ΔNNLO$_{\rm GO}$(450), and to 3% for ΔNNLO$_{\rm GO}$(394). However, we have noticed that the differences between the T-1/D (not shown in Fig. 5) and T-1/T-1 results are of the order of 0.01%, hence negligible. This fact can be understood if we consider an alternative expression for the energy-weighted sum rule. Let us assume we can write the similarity transformed Hamiltonian $\overline{H}_N$ in a tridiagonal form using the Lanczos algorithm [53]. Choosing the vectors

$$\langle w_0| = \frac{\langle 0|\overline{\Theta}_N^\dagger}{\sqrt{\langle 0|\overline{\Theta}_N^\dagger \overline{\Theta}_N|0\rangle}}, \quad |v_0\rangle = \frac{\overline{\Theta}_N|0\rangle}{\sqrt{\langle 0|\overline{\Theta}_N^\dagger \overline{\Theta}_N|0\rangle}} \tag{18}$$

as the left and right pivots, respectively, the energy-weighted sum rule can be calculated as the product between the non-energy-weighted sum rule $m_0 = \langle 0|\overline{\Theta}_N^\dagger \overline{\Theta}_N|0\rangle$ and the first Lanczos coefficient $a_0 = \langle w_0|\overline{H}_N|v_0\rangle$. Because m_0 is a pure ground-state expectation value, it is the same in both the T-1/D and T-1/T-1 schemes. Therefore, triples contributions from the EOM calculation enter in m_1 only via a_0, explaining the small difference between the T-1/D and T-1/T-1 scheme.

Our result for the energy-weighted sum rule can be compared to the Thomas-Reiche-Kuhn (TRK) sum rule, which is often discussed when studying photoabsorption cross sections $\sigma_\gamma(\omega)$ [54]. The TRK sum rule is defined as

$$\int_{\omega_{\rm th}}^{\infty} d\omega\, \sigma_\gamma(\omega) = 5.974 \frac{NZ}{A}\ \text{MeV fm}^2\ (1+\kappa), \tag{19}$$

where $\omega_{\rm th}$ is the threshold energy and κ is the so-called enhancement factor [55]. The latter arises from the presence of exchange terms in the nuclear force, which do not commute with the dipole operator [54]. Considering that $\sigma_\gamma(\omega) = 4\pi^2\alpha\omega R(\omega)$, we can connect m_1 to the left-hand side of Eq. (19) according to

$$\int_{\omega_{\rm th}}^{\infty} d\omega\, \sigma_\gamma(\omega) = 4\pi^2\alpha m_1. \tag{20}$$

Combining Eqs. (19) and (20), we are then able to evaluate the enhancement factor for the employed interactions. Our results for κ, accompanied by our final estimates for m_1, are shown in Table IV. Also in this case uncertainties are obtained summing in quadrature the contributions of (i) and (ii). To be more conservative in the uncertainty estimate, the CC truncation uncertainty (ii) on m_1 has been calculated comparing the T-1/T-1 results directly with the D/D ones, instead of considering the variations between the two best CC schemes available (T-1/T-1 and T-1/D).

We observe that NNLO$_{\rm sat}$ produces the largest value of m_1 and consequently of κ. The three interactions are all consistent in predicting a quite large enhancement factor ranging between 0.9 and 1. This is not surprising as there are components of nonlocality in these interactions, both at the nucleon-nucleon level and at the three-nucleon force level. Large enhancement factors of about 0.6 had already been observed in Ref. [34], where only two-body forces were used.

Further insight on the $E1$ strength function can be obtained looking at the cluster sum rule [56,57]. This quantity is associated with the excitation of a "molecular" dipole degree of freedom, related to the relative motion of two clusters inside the nucleus. Indicating with $(A_i,\ Z_i)$, $i = 1,\ 2$ the mass and proton number of the two clusters, and with $(A,\ Z)$ those of the nucleus, we can connect the TRK sum rule to the cluster sum rule as

$$\int_{\omega_{\rm th}}^{\infty} d\omega \left[\sigma_\gamma(\omega) - \sigma_\gamma^{\rm cl_1}(\omega) - \sigma_\gamma^{\rm cl_2}(\omega)\right] = 5.974 \frac{(Z_1A_2 - Z_2A_1)^2}{AA_1A_2}\ \text{MeV fm}^2\ (1+\kappa). \tag{21}$$

The evaluation of the cluster sum rule becomes particularly interesting for a halo nucleus such as ^{8}He. The latter, in fact, can be modeled as a ^{4}He core, representing the first cluster (cl_1), surrounded by four neutrons, constituting the second cluster (cl_2). By choosing $Z_1 = 2, Z_2 = 0$ and $A = 8$, $A_1 = 4$, $A_2 = 4$ one can compute the right-hand side of Eq. (21) and compare it to the left-hand side, which is obtained by integrating the photoabsorption cross section of ^{8}He and subtracting that of ^{4}He given that $\sigma_\gamma^{\rm cl_2} = 0$.

For the NNLO$_{\rm sat}$ interaction, computing the energy-weighted dipole sum rule of ^{4}He in the CC framework, we obtain 41.9(3) MeV fm^2, which using Eq. (19) yields an enhancement factor of 1.02(2), compatible with the results in Table IV. The cluster sum rule for the NNLO$_{\rm sat}$ interaction becomes then

$$\int_{\omega_{\rm th}}^{\infty} d\omega \left[\sigma_\gamma^{^8{\rm He}}(\omega) - \sigma_\gamma^{^4{\rm He}}(\omega)\right] = 6.0(3)\ \text{MeV fm}^2. \tag{22}$$

By looking at the ratio of the cluster sum rule with respect to the TRK sum rule, we are able to quantify how much of the dipole strength of ^{8}He is given by the relative motion between core and halo. The latter turns out to be approximately 30%, which means that the core-halo relative motion appears to determine around 1/3 of the total $E1$ strength for ^{8}He.

C. Electric dipole polarizability

Finally we turn to our calculations of the electric dipole polarizability α_D for ^{8}He. The latter is related to the inverse-energy weighted sum rule by

$$\alpha_D = 2\alpha \int d\omega\, \frac{R(\omega)}{\omega} = 2\alpha m_{-1}, \tag{23}$$

where m_{-1} is calculated using Eq. (15). This implies that α_D is mainly determined by the low-energy part of the discretized spectrum of Fig. 4, in particular by the first states at about 5 MeV.

In Fig. 6, we show the convergence pattern of α_D with respect to $\hbar\Omega$, in the D/D and T-1/T-1 truncation schemes.

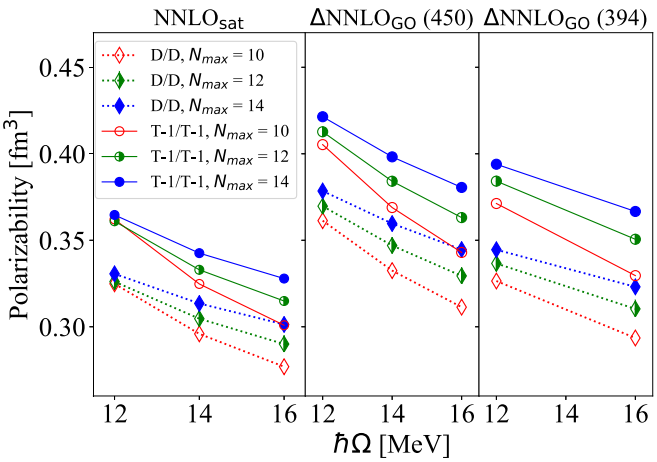

FIG. 6. Dipole polarizability of ^{8}He as a function of the harmonic oscillator frequency $\hbar\Omega$ for the three Hamiltonians, in the D/D and T-1/T-1 truncation schemes.

For all three interactions we observe a quite pronounced dependence of the results on the CC truncation and model space parameters. Variations with respect to $N_{\max}$ tend to reduce in correspondence to small values of the HO frequency. This slow convergence of the polarizability is probably related to the slow convergence of low-lying dipole states.

Triples corrections give a significant contribution to α_D both in the ground- and excited-state part of the CC calculation. For $\hbar\Omega = 12$ MeV, the inclusion of $3p$-$3h$ excitations just in the ground state (T-1/D scheme, not shown in Fig. 6) leads to an increase of α_D between 3 and 5% with respect to the D/D scheme results. If we add triples also in the EOM calculation (T-1/T-1 shown in Fig. 6), we achieve an overall 10% enhancement of the polarizability compared to the full doubles computation. This is different with respect to what is observed for m_1. The reason is that, as shown in Ref. [41], α_D can be rewritten as a continued fraction involving the whole set of Lanczos coefficients available, while m_1 just depends on the first one of them, a_0.

Our final results for the dipole polarizability are reported in Table V. Uncertainties are obtained by summing in quadrature (i) and (ii), where the CC truncation error is computed as the difference between the results of the T-1/T-1 and D/D schemes. Our theoretical uncertainty varies between 7 and 10% of the central value for the different interactions. It is worth noticing that with respect to the other observables previously discussed, we get a more conservative estimate for the uncertainty, which reflects the slow convergence for α_D.

TABLE V. Theoretical predictions for the dipole polarizability of ^{8}He for the three Hamiltonians.

Interaction	α_D (fm^3)
NNLO$_{\rm sat}$	0.37(3)
ΔNNLO$_{\rm GO}$(450)	0.42(3)
ΔNNLO$_{\rm GO}$(394)	0.39(2)

This might be due to the loosely bound halo neutrons in ^{8}He, which determine a more extended wave function, and as a consequence a slower convergence. Finally, the fact that the ΔNNLO$_{\rm GO}$(450) yields the largest prediction for α_D as seen in Table V is related to the dipole strength showing a state at slightly lower energies with respect to the other interactions (see Fig. 4).

Interestingly, our calculations show that the dipole polarizability of ^{8}He is more than five times larger than that of ^{4}He. Combining the photoabsorption cross section data of Refs. [58–60] the latter amounts to 0.074(9) fm^3, which is compatible with the results of Ref. [41]. A larger polarizability is expected in halo nuclei due to soft dipole mode excitations, such as those shown in Fig. 4 at about 5 MeV, which are not seen in ^{4}He [34,41].

IV. CONCLUSIONS

In this paper we carried out a systematic investigation of ground and dipole excited states of the ^{8}He halo nucleus using CC theory and different chiral nucleon-nucleon and three-nucleon forces. We obtain results that are consistent with experiment for the ground-state energy, albeit with a slight underbinding, and the nuclear charge radius. Looking at the three implemented Hamiltonians separately, we see that the Δ-full interaction ΔNNLO$_{\rm GO}$(450) delivers the best agreement with the most recent experimental update of the charge radius of ^{8}He [20].

We also presented the first theoretical predictions for the energy-weighted and inverse energy-weighted sum rules of ^{8}He. From the former we compare the TRK and cluster sum rules to conclude that about 1/3 of the dipole strength is due to the excitation of the molecular dipole degrees of freedom. For the latter, we provide a prediction that could be tested in future experiments. An experimental determination of the dipole strength of ^{8}He, performed with Coulomb excitation at RIKEN in Japan, is currently under analysis [21].

To address the recent theoretical and experimental indications of deformation in the ground state of ^{8}He [11,12] we plan to extend the CC calculations reported in this paper by starting from an axially symmetric reference state following Ref. [61]. We also plan to address EFT truncation errors by performing an order-by-order study of the χEFT uncertainty, supported by Bayesian statistical tools [62].

ACKNOWLEDGMENTS

This work was supported by the Deutsche Forschungsgemeinschaft through Grant No. 279384907–SFB 1245 and through the Cluster of Excellence "Precision Physics, Fundamental Interactions, and Structure of Matter" (PRISMA$^+$ EXC 2118/1, Grant No. 39083149); by the Office of Nuclear Physics, U.S. Department of Energy, under Grant No. DE-SC0018223 (NUCLEI SciDAC-4 collaboration) and Contract No. DE-AC05-00OR22725 with UT-Battelle, LLC (ORNL). Computer time was provided by the Innovative and Novel Computational Impact on Theory and Experiment program and by the supercomputer Mogon at Johannes Gutenberg

Universität Mainz. This research used resources of the Oak Ridge Leadership Computing Facility located at ORNL, which is supported by the Office of Science of the Department of Energy under Contract No. DE-AC05-00OR22725.

[1] I. Tanihata, H. Hamagaki, O. Hashimoto, Y. Shida, N. Yoshikawa, K. Sugimoto, O. Yamakawa, T. Kobayashi, and N. Takahashi, Measurements of Interaction Cross Sections and Nuclear Radii in the Light *p*-Shell Region, Phys. Rev. Lett. **55**, 2676 (1985).

[2] I. Tanihata, T. Kobayashi, O. Yamakawa, S. Shimoura, K. Ekuni, K. Sugimoto, N. Takahashi, T. Shimoda, and H. Sato, Measurement of interaction cross sections using isotope beams of Be and B and isospin dependence of the nuclear radii, Phys. Lett. B **206**, 592 (1988).

[3] K. Blaum, J. Dilling, and W. Nörtershäuser, Precision atomic physics techniques for nuclear physics with radioactive beams, Phys. Scr. **T152**, 014017 (2013).

[4] M. V. Zhukov, B. V. Danilin, D. V. Fedorov, J. M. Bang, I. J. Thompson, and J. S. Vaagen, Bound state properties of borromean halo nuclei: ^{6}He and ^{11}Li, Phys. Rep. **231**, 151 (1993).

[5] G. Hagen, D. J. Dean, M. Hjorth-Jensen, and T. Papenbrock, Complex coupled-cluster approach to an ab-initio description of open quantum systems, Phys. Lett. B **656**, 169 (2007).

[6] S. Bacca, A. Schwenk, G. Hagen, and T. Papenbrock, Helium halo nuclei from low-momentum interactions, Eur. Phys. J. A **42**, 553 (2009).

[7] S. Bacca, N. Barnea, and A. Schwenk, Matter and charge radius of ^{6}He in the hyperspherical-harmonics approach, Phys. Rev. C **86**, 034321 (2012).

[8] P. Maris, J. P. Vary, and P. Navrátil, Structure of $A = 7 - 8$ nuclei with two- plus three-nucleon interactions from chiral effective field theory, Phys. Rev. C **87**, 014327 (2013).

[9] M. A. Caprio, P. Maris, and J. P. Vary, Halo nuclei ^{6}He and ^{8}He with the Coulomb-Sturmian basis, Phys. Rev. C **90**, 034305 (2014).

[10] C. Romero-Redondo, S. Quaglioni, P. Navrátil, and G. Hupin, How Many-Body Correlations and α Clustering Shape ^{6}He, Phys. Rev. Lett. **117**, 222501 (2016).

[11] K. D. Launey, T. Dytrych, G. H. Sargsyan, R. B. Baker, and J. P. Draayer, Emergent symplectic symmetry in atomic nuclei, Eur. Phys. J. Spec. Top. **229**, 2429 (2020).

[12] M. Holl, R. Kanungo, Z. H. Sun, G. Hagen, J. A. Lay, A. M. Moro, P. Navrátil, T. Papenbrock, M. Alcorta, D. Connolly, B. Davids, A. Diaz Varela, M. Gennari, G. Hackman, J. Henderson, S. Ishimoto, A. I. Kilic, R. Krücken, A. Lennarz, J. Liang *et al.*, Proton inelastic scattering reveals deformation in ^{8}He, Phys. Lett. B **822**, 136710 (2021).

[13] F. Coester, Bound states of a many-particle system, Nucl. Phys. **7**, 421 (1958).

[14] F. Coester and H. Kümmel, Short-range correlations in nuclear wave functions, Nucl. Phys. **17**, 477 (1960).

[15] J. Čížek, On the correlation problem in atomic and molecular systems: Calculation of wavefunction components in Ursell-type expansion using quantum-field theoretical methods, J. Chem. Phys. **45**, 4256 (1966).

[16] J. Čížek, On the use of the cluster expansion and the technique of diagrams in calculations of correlation effects in atoms and molecules, in *Advances in Chemical Physics* (Wiley, New York, 2007), pp. 35–89.

[17] H. Kümmel, K. H. Lührmann, and J. G. Zabolitzky, Many-fermion theory in exp S- (or coupled cluster) form, Phys. Rep. **36**, 1 (1978).

[18] R. J. Bartlett and M. Musiał, Coupled-cluster theory in quantum chemistry, Rev. Mod. Phys. **79**, 291 (2007).

[19] G. Hagen, T. Papenbrock, M. Hjorth-Jensen, and D. J. Dean, Coupled-cluster computations of atomic nuclei, Rep. Prog. Phys. **77**, 096302 (2014).

[20] J. J. Krauth, K. Schuhmann, M. A. Ahmed, F. D. Amaro, P. Amaro, F. Biraben, T.-L. Chen, D. S. Covita, A. J. Dax, M. Diepold, L. M. P. Fernandes, B. Franke, S. Galtier, A. L. Gouvea, J. Götzfried, T. Graf, T. W. Hänsch, J. Hartmann, M. Hildebrandt, P. Indelicato *et al.*, Measuring the α-particle charge radius with muonic helium-4 ions, Nature (London) **589**, 527 (2021).

[21] T. Aumann (private communication).

[22] E. Epelbaum, H.-W. Hammer, and Ulf-G. Meißner, Modern theory of nuclear forces, Rev. Mod. Phys. **81**, 1773 (2009).

[23] R. Machleidt and D. R. Entem, Chiral effective field theory and nuclear forces, Phys. Rep. **503**, 1 (2011).

[24] H. W. Hammer, S. König, and U. van Kolck, Nuclear effective field theory: Status and perspectives, Rev. Mod. Phys. **92**, 025004 (2020).

[25] A. Ekström, G. Baardsen, C. Forssén, G. Hagen, M. Hjorth-Jensen, G. R. Jansen, R. Machleidt, W. Nazarewicz, T. Papenbrock, J. Sarich, and S. M. Wild, Optimized Chiral Nucleon-Nucleon Interaction at Next-To-Next-To-Leading Order, Phys. Rev. Lett. **110**, 192502 (2013).

[26] A. Ekström, G. R. Jansen, K. A. Wendt, G. Hagen, T. Papenbrock, B. D. Carlsson, C. Forssén, M. Hjorth-Jensen, P. Navrátil, and W. Nazarewicz, Accurate nuclear radii and binding energies from a chiral interaction, Phys. Rev. C **91**, 051301(R) (2015).

[27] N. Kaiser, S. Gerstendörfer, and W. Weise, Peripheral nn-scattering: Role of delta-excitation, correlated two-pion and vector meson exchange, Nucl. Phys. A **637**, 395 (1998).

[28] H. Krebs, E. Epelbaum, and U. G. Meißner, Nuclear forces with Δ excitations up to next-to-next-to-leading order, part i: Peripheral nucleon-nucleon waves, Eur. Phys. J. A **32**, 127 (2007).

[29] E. Epelbaum, H. Krebs, and U.-G. Meißner, Δ-excitations and the three-nucleon force, Nucl. Phys. A **806**, 65 (2008).

[30] M. Piarulli, L. Girlanda, R. Schiavilla, R. N. Pérez, J. E. Amaro, and E. R. Arriola, Minimally nonlocal nucleon-nucleon potentials with chiral two-pion exchange including Δ resonances, Phys. Rev. C **91**, 024003 (2015).

[31] A. Ekström, G. Hagen, T. D. Morris, T. Papenbrock, and P. D. Schwartz, Δ isobars and nuclear saturation, Phys. Rev. C **97**, 024332 (2018).

[32] W. G. Jiang, A. Ekström, C. Forssén, G. Hagen, G. R. Jansen, and T. Papenbrock, Accurate bulk properties of nuclei from $a = 2$ to ∞ from potentials with Δ isobars, Phys. Rev. C **102**, 054301 (2020).

[33] S. Bacca, N. Barnea, G. Hagen, G. Orlandini, and T. Papenbrock, First Principles Description of the Giant Dipole Resonance in ^{16}**O**, Phys. Rev. Lett. **111**, 122502 (2013).

[34] S. Bacca, N. Barnea, G. Hagen, M. Miorelli, G. Orlandini, and T. Papenbrock, Giant and pigmy dipole resonances in ^{4}He, ^{16,22}O, and ^{40}Ca from chiral nucleon-nucleon interactions, Phys. Rev. C **90**, 064619 (2014).

[35] M. Miorelli, S. Bacca, G. Hagen, and T. Papenbrock, Computing the dipole polarizability of ^{48}Ca with increased precision, Phys. Rev. C **98**, 014324 (2018).

[36] G. Hagen, T. Papenbrock, D. J. Dean, A. Schwenk, A. Nogga, M. Włoch, and P. Piecuch, Coupled-cluster theory for three-body Hamiltonians, Phys. Rev. C **76**, 034302 (2007).

[37] R. Roth, S. Binder, K. Vobig, A. Calci, J. Langhammer, and P. Navrátil, Medium-Mass Nuclei with Normal-Ordered Chiral $NN+3N$ Interactions, Phys. Rev. Lett. **109**, 052501 (2012).

[38] J. F. Stanton and R. J. Bartlett, The equation of motion coupled-cluster method: A systematic biorthogonal approach to molecular excitation energies, transition probabilities, and excited state properties, J. Chem. Phys. **98**, 7029 (1993).

[39] V. D. Efros, W. Leidemann, and G. Orlandini, Response functions from integral transforms with a Lorentz kernel, Phys. Lett. B **338**, 130 (1994).

[40] V. D. Efros, W. Leidemann, G. Orlandini, and N. Barnea, The Lorentz integral transform (lit) method and its applications to perturbation-induced reactions, J. Phys. G **34**, R459(R) (2007).

[41] M. Miorelli, S. Bacca, N. Barnea, G. Hagen, G. R. Jansen, G. Orlandini, and T. Papenbrock, Electric dipole polarizability from first principles calculations, Phys. Rev. C **94**, 034317 (2016).

[42] J. D. Watts, J. Gauss, and R. J. Bartlett, Coupled-cluster methods with noniterative triple excitations for restricted open-shell Hartree-Fock and other general single determinant reference functions. energies and analytical gradients, J. Chem. Phys. **98**, 8718 (1993).

[43] J. D. Watts and R. J. Bartlett, Economical triple excitation equation-of-motion coupled-cluster methods for excitation energies, Chem. Phys. Lett. **233**, 81 (1995).

[44] G. R. Jansen, M. D. Schuster, A. Signoracci, G. Hagen, and P. Navrátil, Open *sd*-shell nuclei from first principles, Phys. Rev. C **94**, 011301(R) (2016).

[45] J. Simonis, S. Bacca, and G. Hagen, First principles electromagnetic responses in medium-mass nuclei: Recent progress from coupled-cluster theory, Eur. Phys. J. A **55**, 241 (2019).

[46] M. Brodeur, T. Brunner, C. Champagne, S. Ettenauer, M. J. Smith, A. Lapierre, R. Ringle, V. L. Ryjkov, S. Bacca, P. Delheij, G. W. F. Drake, D. Lunney, A. Schwenk, and J. Dilling, First Direct Mass Measurement of the Two-Neutron Halo Nucleus ^{6}He and Improved Mass for the Four-Neutron Halo ^{8}He, Phys. Rev. Lett. **108**, 052504 (2012).

[47] E. Tiesinga, P. J. Mohr, D. B. Newell, and B. N. Taylor, Codata recommended values of the fundamental physical constants: 2018, Rev. Mod. Phys. **93**, 025010 (2021).

[48] A. A. Filin, V. Baru, E. Epelbaum, H. Krebs, D. Möller, and P. Reinert, Extraction of the Neutron Charge Radius from a Precision Calculation of the Deuteron Structure Radius, Phys. Rev. Lett. **124**, 082501 (2020).

[49] A. Ong, J. C. Berengut, and V. V. Flambaum, Effect of spin-orbit nuclear charge density corrections due to the anomalous magnetic moment on halonuclei, Phys. Rev. C **82**, 014320 (2010).

[50] G. Papadimitriou, A. T. Kruppa, N. Michel, W. Nazarewicz, M. Płoszajczak, and J. Rotureau, Charge radii and neutron correlations in helium halo nuclei, Phys. Rev. C **84**, 051304(R) (2011).

[51] P. Mueller, I. A. Sulai, A. C. C. Villari, J. A. Alcántara-Núñez, R. Alves-Condé, K. Bailey, G. W. F. Drake, M. Dubois, C. Eléon, G. Gaubert, R. J. Holt, R. V. F. Janssens, N. Lecesne, Z.-T. Lu, T. P. O'Connor, M.-G. Saint-Laurent, J.-C. Thomas, and L.-B. Wang, Nuclear Charge Radius of ^{8}He, Phys. Rev. Lett. **99**, 252501 (2007).

[52] M. S. Golovkov, L. V. Grigorenko, G. M. Ter-Akopian, A. S. Fomichev, Yu.Ts. Oganessian, V. A. Gorshkov, S. A. Krupko, A. M. Rodin, S. I. Sidorchuk, R. S. Slepnev, S. V. Stepantsov, R. Wolski, D. Y. Pang, V. Chudoba, A. A. Korsheninnikov, E. A. Kuzmin, E. Yu. Nikolskii, B. G. Novatskii, D. N. Stepanov, P. Roussel-Chomaz *et al.*, The ^{8}He and ^{10}He spectra studied in the (t, p) reaction, Phys. Lett. B **672**, 22 (2009).

[53] C. Lanczos, An iteration method for the solution of the eigenvalue problem of linear differential and integral operators, J. Res. Nat. Bur. Stand. **45**, 255 (1950).

[54] G. Orlandini and M. Traini, Sum rules for electron-nucleus scattering, Rep. Prog. Phys. **54**, 257 (1991).

[55] J. M. Eisenberg and W. Greiner, *Nuclear Theory: Excitation Mechanisms of the Nucleus* (North-Holland Publishing Co., Netherlands, 1976), Vol. 2.

[56] Y. Alhassid, M. Gai, and G. F. Bertsch, Radiative Width of Molecular-Cluster States, Phys. Rev. Lett. **49**, 1482 (1982).

[57] K. Hencken, G. Baur, and D. Trautmann, A cluster version of the ggt sum rule, Nucl. Phys. A **733**, 200 (2004).

[58] Y. M. Arkatov, P. I. Vatset, V. I. Voloshchuk, V. A. Zolenko, I. M. Prokhorets, and V. I. Chimil, Energy moments of the γ-ray total-absorption cross section of ^{4}He, Sov. J. Nucl. Phys. **19**, 598 (1975).

[59] Yu. M. Arkatov, P. I. Vatset, V. I. Voloshchuk, V. A. Zolenko, and I. M. Prokhorets, Experimental verification of the sum rules for photodisintegration of ^{4}He, Sov. J. Nucl. Phys. **31**, 726 (1980).

[60] K. Pachucki and A. M. Moro, Nuclear polarizability of helium isotopes in atomic transitions, Phys. Rev. A **75**, 032521 (2007).

[61] S. J. Novario, G. Hagen, G. R. Jansen, and T. Papenbrock, Charge radii of exotic neon and magnesium isotopes, Phys. Rev. C **102**, 051303(R) (2020).

[62] R. J. Furnstahl, D. R. Phillips, and S. Wesolowski, A recipe for EFT uncertainty quantification in nuclear physics, J. Phys. G **42**, 034028 (2015).